Müller cells separate between wavelengths to improve day vision with minimal effect upon night vision

Amichai M. Labin [1,2*] , Shadi K.Safuri [2*] , Erez N. Ribak [1] and Ido Perlman [2]

[1] Department of Physics, Technion - Israel Institute of Technology, Haifa 32000, Israel

[2] Department of Physiology and Biophysics, Ruth & Bruce Rappaport Faculty of Medicine, Technion - Israel Institute of Technology and Rappaport Institute, Haifa 31096, Israel

* These Authors contributed equally to this work.

Vision starts with the absorption of light by the retinal photoreceptors - cones and rods. However, due to the 'inverted' structure of the retina, the incident light must propagate through reflecting and scattering cellular layers before reaching the photoreceptors. It has been recently suggested that Müller cells function as optical fibers in the retina, transferring light illuminating the retinal surface onto the cone photoreceptors. Here we show that Müller cells are wavelength-dependent wave-guides, concentrating the green-red part of the visible spectrum onto cones and allowing the blue-purple part to leak onto nearby rods. This phenomenon is observed in the isolated retina and explained by a computational model, for the guinea pig and the human parafoveal retina. Therefore, light propagation by Müller cells through the retina can be considered as an integral part of the first step in the visual process, increasing photon absorption by cones while minimally affecting rod-mediated vision.

The primary event of vision is the projection of light by the optical system of the eye onto the proximal surface of the retina[1]. However, the mammalian retina and the peripheral retina of humans and primates are organized in a seemingly reverse order with respect to the light path. This arrangement places the photoreceptors, responsible for light absorption[2,3] _ENREF_2 _ENREF_2, as the last cells in the path of light, rather than the first[4,5] _ENREF_1. Therefore, the incident light must propagate through five reflecting and scattering layers of cell bodies and neural processes before reaching the photoreceptors. This "inverted" retinal structure is expected to cause blurring of the image and reduction in the photon flux reaching the photoreceptors, thus reducing their sensitivity[6,7,8,9]. It has been recently reported that retinal Müller cells act as light guides serving to transfer light across the retina, from the vitreo-retinal border towards the photoreceptors[10,11,12]. However, the basic question remains: How does light propagation via Müller cells through the neuronal layers of the retina affect vision?

A single Müller cell collects light at the vitreo-retinal surface from an extended retinal region, and guides it onto one coupled cone, located at its distal end[13] (Fig. 1a). Since the proximal, receiving end of the Müller cell is wide, compared to its distal part, and covers also ~15 rods surrounding the central cone (Fig. 1a), any light concentration into the cone is expected to reduce the light reaching the rods and impede rod-mediated vision, crucial for dark conditions[14]. On the other hand, if light guiding onto cones is ineffective, cone-mediated vision, crucial for day-time conditions, will suffer from a substantial loss of sensitivity as a result of light scattering by the neuronal retina. Can this cost-benefit optimization problem between day vision and night vision be solved, without significantly impeding one of the two?

Results

Role of Müller cells in light propagation through the retina: computational analysis

As a first step in addressing the above question, we performed light propagation simulation for monochromatic light through the peripheral human retina. Using previously measured refractive index profile, obtained by phase microscopy measurements

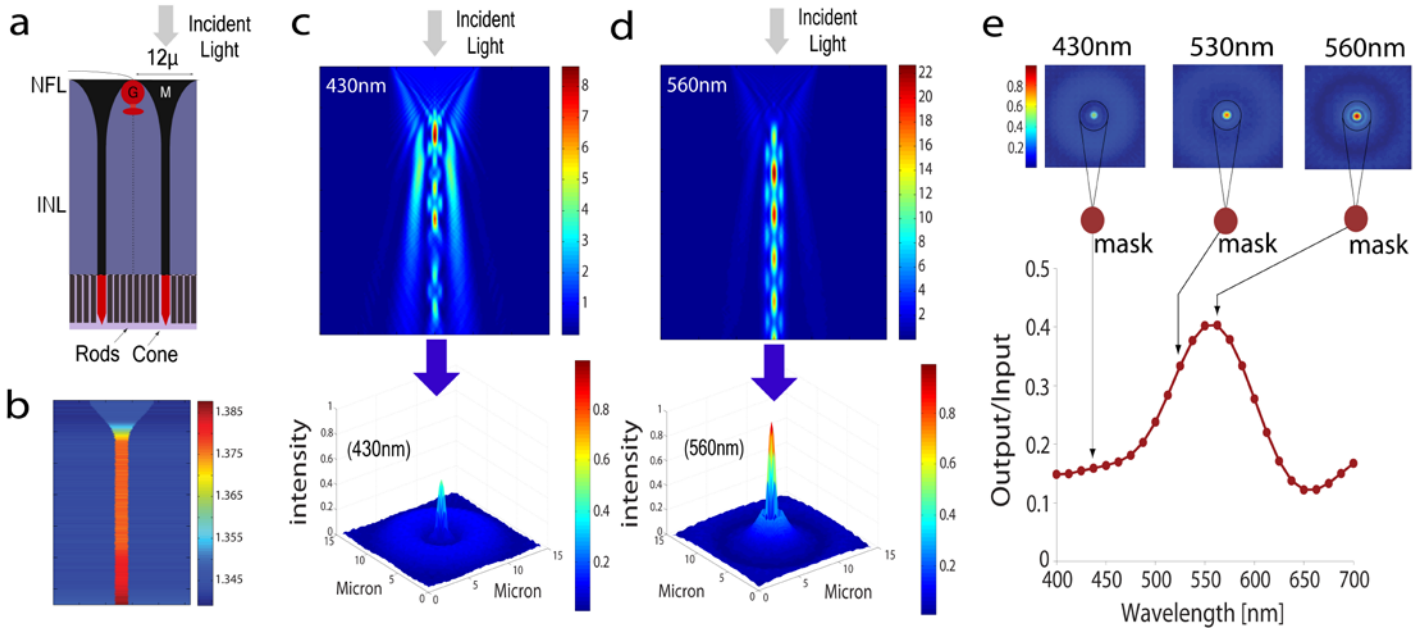

Fig. 1. (a) Schematic representation of Müller cells and photoreceptors organization in the human parafoveal retina. Müller cells' (in black) proximal cup-like funnel of ~12 µm in diameter, covers ~15 rods in addition to the central cone. (b) A data cube of 1000×256×256 grid containing a Müller cell (of ~130 µm length) and its surrounding tissue was reconstructed, based upon measured indices of refraction profile (scale on the right). (c-d) Simulation of light passing through a single Müller cell (top) and the corresponding distribution at the distal part of the cell (bottom), for an incident light of 430 nm (blue) and 560 nm (green-yellow). Light concentration into the center (cone's receptive field) is higher for the green than for the blue. (e) The transmitted spectrum into the central cone is calculated by summing the pixels inside the Müller cell's area, and averaged over the last longitudinal intensity cycle. The peak transmission is at 560 nm, corresponding for the green-yellow part of the visible spectrum.

of human retinas[10], we reconstructed a 1000×256×256 data-cube grid, which contains a Müller cell and its vicinity in the human parafoveal retina[15,16] (Fig. 1b). In order to calculate light propagation through the Müller data-cube, we have developed[11] and applied a known algorithm, the Fast Fourier Transform Beam Propagation Method (FFT BPM)[17,18,19,20,21]. This is a direct three-dimensional numerical solution of the wave equation, also known as the scalar Helmholtz equation[22,23]:

$$\nabla^2 E(\bar{r}) + k^2 n^2(\bar{r}) E(\bar{r}) = 0 \qquad (1)$$

Here $E(\bar{r})$ is the light propagating field and $\bar{r} = (x, y, z)$, where z is the propagation direction (across the retina). $k = 2\pi / \lambda$, where λ is the light wavelength. $n(\bar{r})$ is the refractive index profile of the retina, and $\nabla^2 = \partial^2 / \partial x^2 + \partial^2 / \partial y^2 + \partial^2 / \partial z^2$ is the three dimensional derivative, the laplacian (see also Supplementary Information). An initial light distribution entering the cell was taken as a diffraction pattern from the eye's pupil, which is broadened by corneal aberrations, to create an average Gaussian distribution of ~40 μm width[24,25]. Next, the field was propagated down the medium, plane by plane, where every step was of 0.13 μm length.

In order to test how robust was our simulation procedure, we introduced fluctuations in several parameters of the above simulation procedure (see Supplementary Information): (1) Müller cells *in vivo* do not appear as straight "nail-like" structure, as illustrated in Fig. 1a, but rather show some bending. We use 20 random bending realizations and derive for each its wavelength properties as a wave-guiding element. (2) Perturbations were added randomly up to 5% of the cell's width[15] in order to simulate the uneven boundaries and undulations of the cells. (3) We also added random perturbations (Fig. 1b) of the cell's refractive indices and its extracellular vicinity[26], on a scale of 1 μm and ~5% of the local refractive index, to simulate scattering by adjacent nuclear layers. The results of the simulations are robust (see Supplementary Information), and show that Müller cells efficiency as light guides varies with wavelength. Representative light distributions, propagating through a Müller cell for blue (430 nm) and green-yellow (560 nm) wavelengths can be seen in figures 1c and 1d respectively. The maximum output intensity of the green-yellow light distribution is nearly twice the corresponding blue light maximum (Fig. 1c-d-bottom). We carried out light propagation analysis through Müller cells in the human parafoveal retina for 25 distinct wavelengths spanning the visible spectrum (400 nm – 700 nm). For each output light distribution, the intensity inside a circle mask (Fig. 1e) was summed to obtain the transmitted intensity into the central cone. To avoid the influence of the periodic intensity along the cells (Fig. 1c-d) we averaged it over the last cycle. The results for the entire visible spectrum (Fig. 1e) show that the maximum guiding efficiency occurs for green-yellow light (560 nm). This light is concentrated onto the center – the cone receptive field area. In contrast, violet-blue light leaks outside the Müller cells to where the surrounding rods are located. To quantify the spectral effect by Müller cells, we defined a

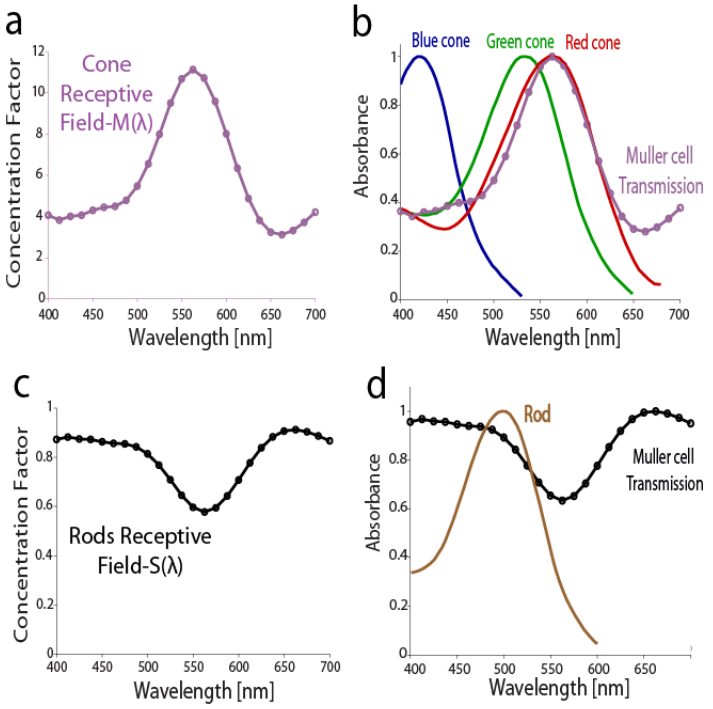

Fig. 2. (a) Light concentration factor, $M(\lambda)$, exhibits a wavelength-dependent enhancement with a maximum of ×11 for 560 nm. (b) Normalized light intensity tunneling inside a Müller cell (purple circles) is compared to the normalized absorbance spectra of the three spectral types of human cone photoreceptors[3,25,26] _ENREF_2. (c) Calculated spectrum of light leaking out of the Müller cells and illuminating the surrounding area, normalized by a uniform illumination, $S(\lambda)$. The intensity is reduced by a maximum of ~40% at ~560 nm, while for blue (λ<500 nm) light the reduction is only by ~15%. (d) Normalized light intensity leaking out of Müller cells (black circles) is compared to normalized rods' absorbance spectrum[25].

concentration factor for light in the center of the Müller cell $M(\lambda)$ and in its surrounding space $S(\lambda)$. The concentration factor is the mean intensity of guided light, normalized by the mean intensity of a uniform illumination. This quantity is a ratio between the number of photons reaching a photoreceptor by Müller cell, and the number of photons that would have reached it in a free propagation.

The calculated results show that light concentration is wavelength dependent and $M(\lambda)$ has a maximum of ~11 at 560 nm (Fig. 2a). This means that the number of 560 nm photons reaching a single cone is 11 times larger due to Müller cells optical effect, compared to the situation in which light incident upon the retinal surface would have propagated freely through the retina. The spectrum of light transmitted by Müller cells (Fig. 2b) is remarkably similar to the measured spectral absorbance of human long-wavelength cones (L-cones)[27,28,29] and closely overlaps with that of medium-wavelength cones (M-cones), as shown in figure 2b. Interestingly, this result is consistent with the natural abundance of L- and M-cones, which accounts together for ~90% of all cones[4,30]. As a result of the cup-like structure (endfoot) of the most proximal portion of Müller cell, red-green light impinging upon the retina is being gathered from a large retinal region of ~20 photoreceptors, and concentrated onto a single central cone[13]. Consequently, a reduced light intensity propagates in the surrounding area, corresponding to the rods' receptive fields. Therefore, the intensity of light in the green-red band (520-600 nm) reaching the rods is lowered by 30-40% (Fig. 2c), but only by 5-15% for the blue region of the spectrum (λ<500 nm), a region to which rods are more sensitive (Fig. 2d). When light enters the pupil away from its center, it reaches the retina as a tilted wavefront, rather than perpendicularly. At night time, the pupil dilates up to 8 mm, and with an average eye length of 23 mm, the maximum incidence angle with respect to the retina is ~10^0. Therefore, we calculated also the average transmission of light in the Müller waveguide cells for light entering the eye at an incident slant of up to $10^{0,}$ and found the same peak transmission wavelength of 560 nm (See Supplementary Information).

The results of the optical simulations suggest that when white light is focused upon the surface of the peripheral human retina, it is being spectrally separated by Müller cells; the green-red part of the spectrum is concentrated by up to one order of

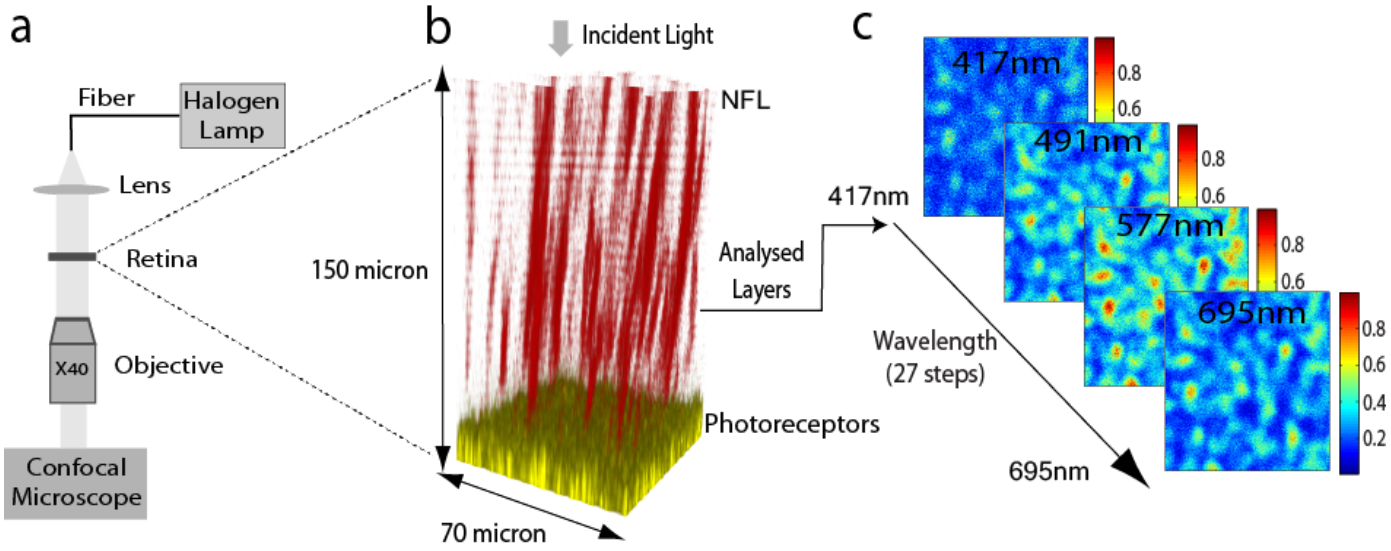

Fig. 3. (a) Light from a halogen lamp is injected into an optical fiber, collimated onto the retina and imaged by a confocal microscope. (b) Light transmission through the retina is reconstructed in 3D (obtained by the microscope's Z-axis stack). Distinct light tubes of high transmission - the red channel (588 nm wavelength), spanning 150 μm, from the retinal surface to just above the photoreceptor layer are observed. The yellow channel is the auto-fluorescence track, used to locate photoreceptors outer segments. For this purpose, the stack was obtained using a long working distance lens. (c) Above the level of photoreceptors, the transmitted light is imaged using the microscope's spectral mode. The 417 nm - 695 nm range is covered by 27 distinct images at intervals of 10 nm. Four representative images for different wavelength (417 nm, 491 nm, 577 nm and 695 nm) are shown.

magnitude onto the cone photoreceptors and at the same time, light reaching the rods is reduced only by 5-15% for wavelengths shorter than 500 nm (Fig. 2c-d). Thus, Müller cells are dividing the visible spectrum in a manner that augments the cone's light absorption, while reducing minimally light absorption by the surrounding rods.

The above computational analysis was conducted for the human peripheral retina, and should also apply to other diurnal species. For nocturnal species another mechanism has been suggested, in which an inverted rod nuclei act as collecting lenses [31,32], directing light onto the rod's outer segments.

Optical role of Müller cells in the guinea pig retina: experimental and computational analysis

In order to examine experimentally the conclusions of the above computational analysis, we recorded the spatial and spectral distribution of light, propagating through the guinea pig retina, following by an illumination on the retinal surface, at the ganglion cells side, by a halogen light source (broad spectral source). We chose the guinea pig retina since its retinal refractive index profile and dimensions of Müller cells are known[10,15]. Thus, the above optical calculations can also be conducted and compared to the experimental results. A piece of a guinea pig retina was isolated from the pigment epithelium and was mounted on the stage of an inverted confocal microscope with photoreceptors facing the objective. Prior to recording, we identified the level of photoreceptors outer segments in order to assure that imaging was not taken within the photoreceptors

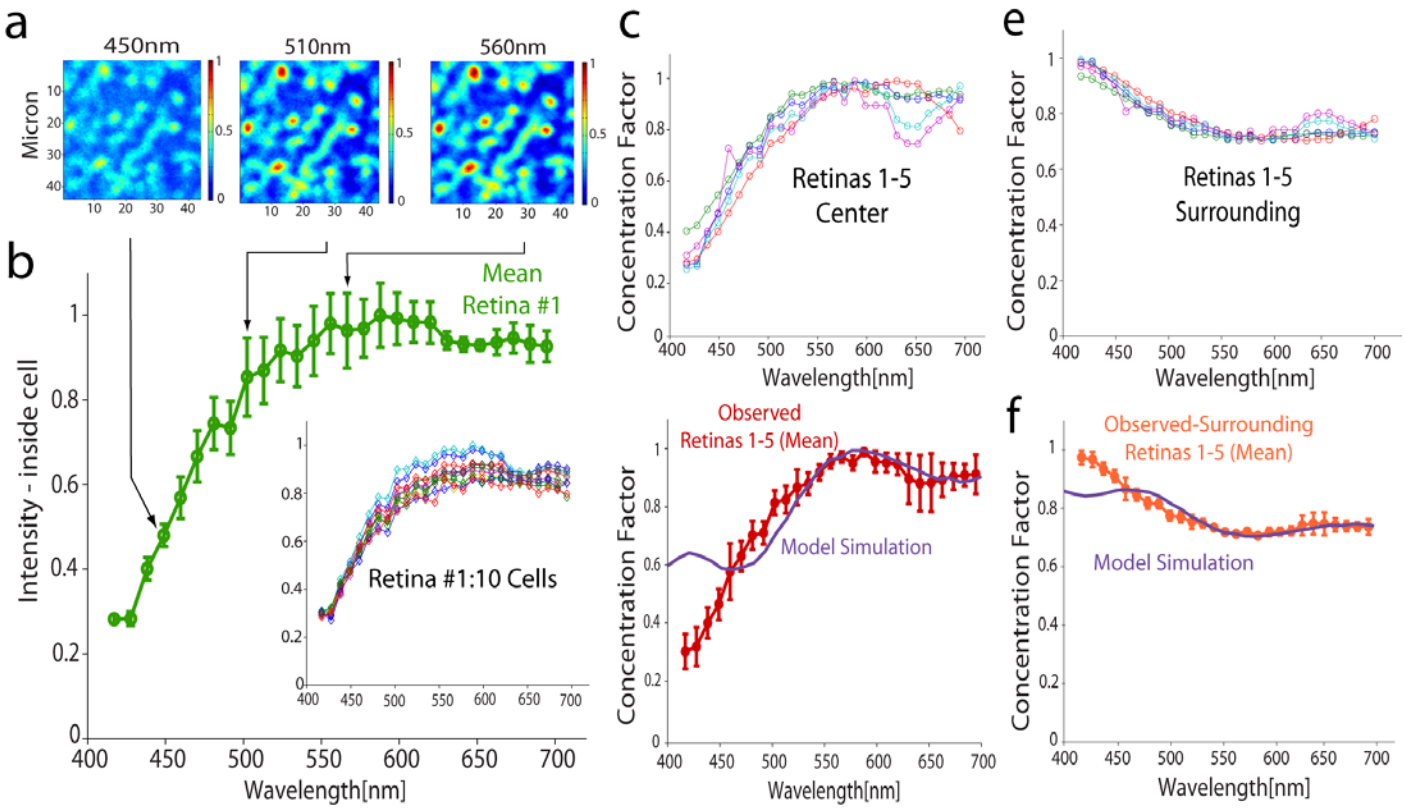

Fig. 4. (a) Twenty seven images of transmitted light were recorded above the photoreceptors layer. Three representative images for short- (450nm), middle- (510nm) and long- (560nm) wavelengths are shown. The images were normalized (the sum of all pixels is equal for all images). Müller cells light tubes were located by a threshold and the 10 highest transmission cells were marked and masked. All these cells, without exception, show a higher transmission of red-green wavelengths (b - inset). (b) Mean (± sd) of the spectral light distribution inside Müller cells (N = 10), studied in the guinea pig retina #1. (c) Light concentration spectra inside Müller cells (different colors), and in their surrounding areas (e) were obtained from five different retinal preparations. The mean (± sd) of the concentration spectra of light transmitted inside Müller cells, and in their surrounding in all studied retinas (N = 5) correspond well with the concentration spectra obtained using the model simulation (purple curve) (d and f respectively).

layers, but at a more proximal level where Müller cells are located. For that purpose, we utilized the observation that the photoreceptors outer segments are the source of the most intense auto-fluorescence[27,33] within the retina, and identified the outer segment depth from the retinal surface (see Supplementary Information). Then, the microscope configuration was switched to record the spectral transmission of light in the retina (Fig. 3a). Images of transmitted light were recorded at optical sections of 5 µm thickness spanning a total of 150 µm, corresponding to the average length of Müller cells, from distal to proximal ends. We could clearly identify distinct light guiding tubes across most of the retinal depth (Fig. 3b, in red), spanning the retina from the retinal surface down to just above the photoreceptors. The only retinal structures that fit these light-guiding tubes are the Müller cells.

In order to measure the spectral properties of light transmitted by Müller cells, we identified the high transmission areas ("hot spots") in the recorded images, taken above the photoreceptors layer. These images form a set of 27 channels which covers the visible range (417-695 nm). Four representative images of four distinct spectral channels are shown in Fig. 3c.

In order to quantify the spectrum of the guided light within Müller cells, we summed the pixel intensity inside the cells' areas for the 27 monochromatic images (see three representative images of examined retina #1, Fig. 4a). Next, we normalized the intensities of these 27 channels relative to the intrinsic halogen light source spectrum (see Supplementary Information). The spectral distributions of light transmitted inside 10 Müller cells (Fig. 4b, inset) show clear enhancement for wavelengths in the red-green region of the visible spectrum in comparison to the blue-violet spectral band. The mean light intensity propagating inside these 10 Müller cells, studied in retina #1, reaches its peak at ~575 nm, and decreases towards shorter wavelengths and longer wavelengths (Fig. 4b).

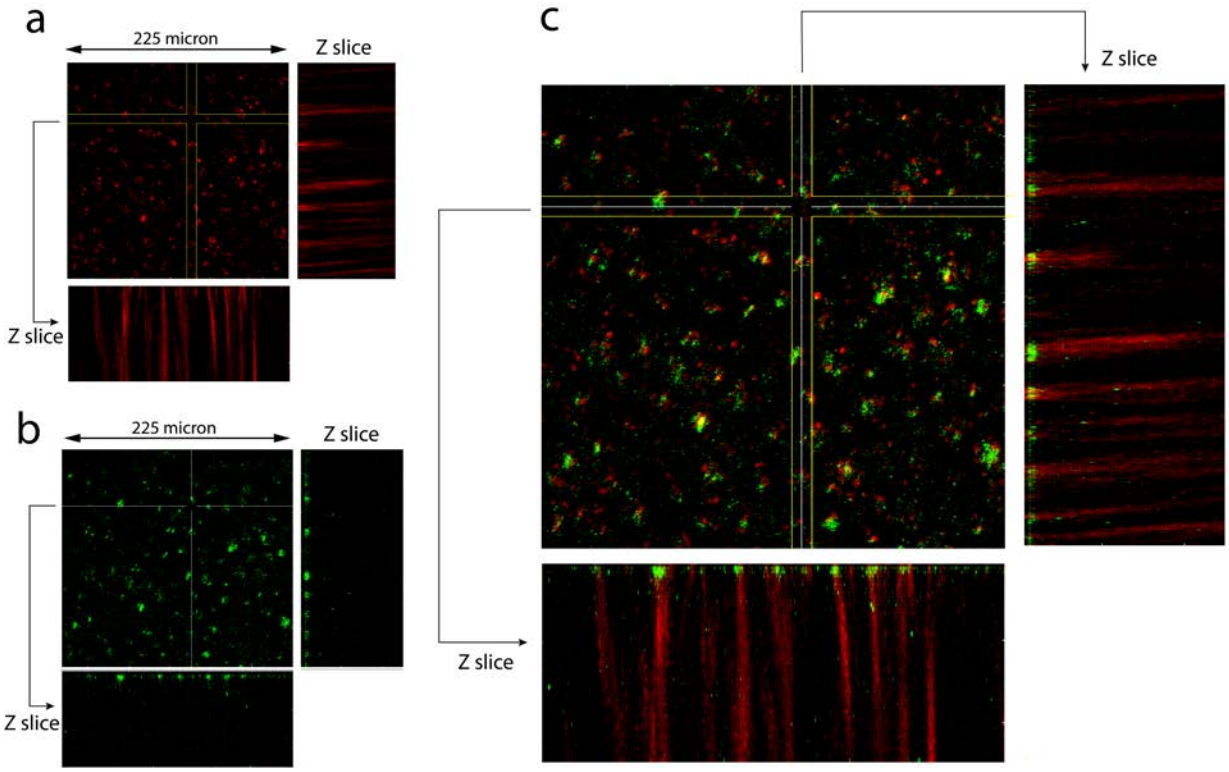

Fig. 5: (a) Transmission channel (in red), recorded after 617 nm LED illumination from the retinal surface (ganglion cells side). (b) Reflection channel (in green), obtained by cone selective dye (FITC-PNA), and recorded by fluorescence scheme after 488 nm laser illumination from the photoreceptors side. (c) Merge of the two channels at the photoreceptors layer and in orthogonal Z slices. The Muller cells light guiding tubes are aligned with the fluorescence green signal emitted from the labeled cones.

Similar experiments were conducted in five different experimental sessions on retinas from five guinea pigs, and the resultant average spectra of light transmitted within Müller cells in these five retinas (Fig. 4c) show minor variations. The average spectrum of light transmitted inside Müller cells of all five guinea pigs (red curve, Fig. 4d) shows remarkable agreement with the corresponding calculated spectrum, obtained by the optical simulation that was performed for the guinea pig retina (purple curve, Fig. 4d). We also analyzed the spectral distribution of light leakage, by measuring light outside the hot spot areas of Müller cells. The light reaching the surroundings of Müller cells also showed wavelength dependency, as illustrated by the mean spectra of the five retinas (Fig. 4e). The measured average spectrum (orange curve, Fig. 4f) corresponds well with the calculated wavelength dependency of light leaking outside Müller cells as obtained by the optical simulation (purple curve, Fig. 4f). A difference can be seen between the experimental spectra and the calculated ones within the short-wavelengths range (400-450 nm), for light transmitted inside Müller cells and for light leaking outside the cells (Figs. 4d and 4f respectively). This may result from small density fluctuations in the cells, within the path of light. These short scale fluctuations[26] generate Rayleigh scattering of the far blue wavelengths, which cannot be simulated in the framework of Beam Propagation Methods (BPM). It should be noted that guinea pig retina contains rods with visual pigment absorbing maximally at 500 nm and two types of cones; a short-wavelength cone (S-cone) with maximal absorption at 400 nm and a medium-wavelength cone (M-cone) with peak absorption at 530 nm[34]. Thus, light concentration by Müller cells increases photon absorption by the distal cones, but the photon gain effect is smaller compared to the effects of Müller cells upon S-, M- and L-cones of the human equivalent. (See Supplemental Information).

Spatial co-alignment between cone photoreceptors and Müller cells light guides

To assure that the recorded light guiding tubes are directed each into a single cone photoreceptor and not randomly coupled to the photoreceptors layer, we measured the correlation between cones and light guiding tubes. For that purpose, prior to optical recording, cone photoreceptors were selectively labeled by FITC-PNA dye[35] (See Supplementary Information). Then, we used the multi-track mode of the confocal microscope to obtain reflection (FITC) and transmission recordings sequentially. The optical configuration was identical to the configuration we describe above for all of our experiments. However, for the transmission recording we illuminated the retina surface (ganglion cells side) with a 617 nm light emitting diode (LED) instead of the halogen lamp, to avoid a situation in which the guided light would excite the cones' dye and contaminate the transmission channel. We obtained stacks spanning 100 µm (50 optical slices, each 2 µm) above the photoreceptors layer. Orthogonal views of the transmission channel (Fig. 5a), reflection channel (Fig. 5b) and both channels superimposed (Fig. 5c) show a clear spatial association between the cones reflection and Müller cells light guiding transmission tubes. We performed quantitative analysis by thresholding both channels, at the photoreceptors layer, and comparing high intensity areas. We found that all Müller cells were coupled to a single cone each and at least 89% of all cones were coupled to Müller cells.

Photon absorption by the photoreceptors due to Müller cells spectral splitting

In order to assess the effects of Müller cells spectral separation on photon absorption by cone- and rod-photoreceptors in the human parafoveal retina, we calculated light absorbance in cones' outer segments, $A_{Cone}(\lambda)$ by multiplying the Müller cell's concentration factor, $M(\lambda)$ (Fig. 2a) by the normal cone absorbance profile- $C(\lambda)$, such that $A_{Cone}(\lambda) = M(\lambda)C(\lambda)$ (Fig. 6a-c). Photon absorption in rods' outer segments $A_{Rod}(\lambda)$ was similarly calculated by multiplying the spectrum of light leaking outside the Müller cell into the surrounding area $S(\lambda)$ (Fig. 2c), by the absorption spectrum of the rod visual pigment $R(\lambda)$, $A_{Rod}(\lambda) = S(\lambda)R(\lambda)$ (Fig. 6d). We found that the gain in photon absorption for white light impinging upon the retinal surface and propagating across the retina by the Müller cells, $\sum_{\lambda} A(\lambda) / \sum_{\lambda} C(\lambda)$, showed an increase by a factor of ~7.5 for the L- and M-cones, and by a factor of ~4 for the S-cones (Fig. 6e). On the other hand, Müller cells' properties cause loss in photon absorption by rods, but only by 20% (Fig. 6e).

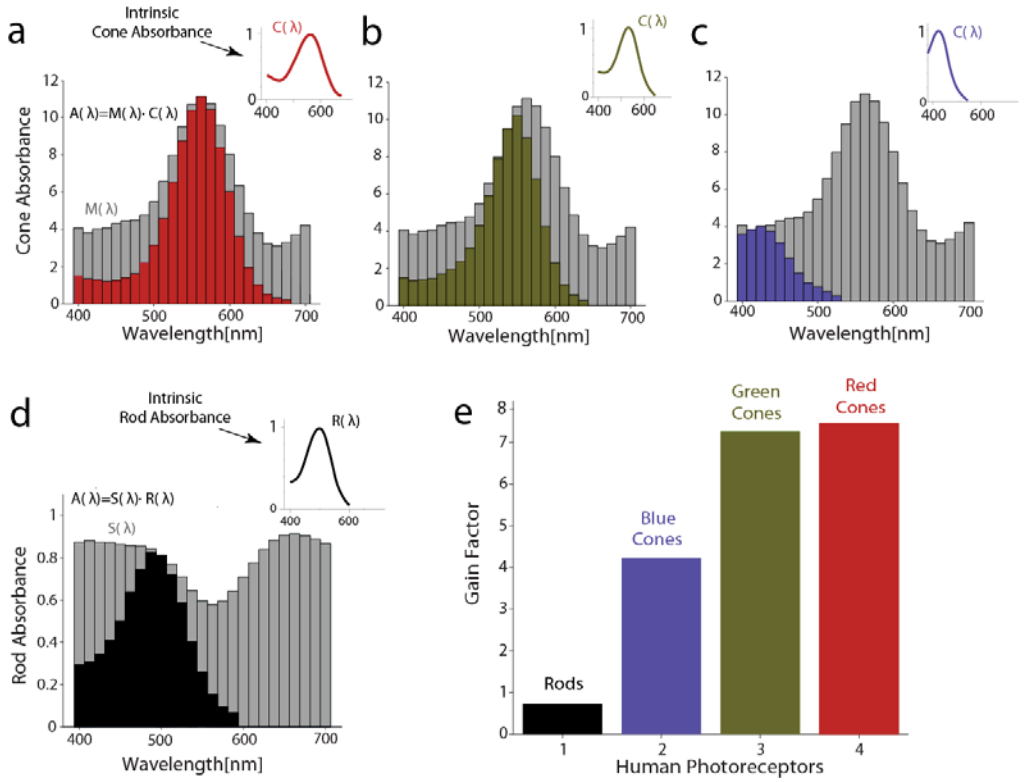

Fig. 6. Gain in photoreceptors light absorption in the human parafoveal retina, due to Müller cells' spectral separation. (a-c) The Müller cell light concentration into cones - $M(\lambda)$ (in gray bars), multiplied by the absorption spectrum of the cone visual pigment ($C(\lambda)$, line curves) results in the gain of cone absorption $A_{Cone}(\lambda) = M(\lambda)C(\lambda)$ (red, green and blue respectively). (d) Light transmission outside Müller cells and illuminating rods - $S(\lambda)$ (in gray bars), multiplied by the absorption spectrum of rod visual pigment - $R(\lambda)$, results in the gain of rod absorption (black). (e) The total light absorption in cones is increased by Müller cells' light concentration. The gain is highest for long-wavelength cones, slightly lower for the middle-wavelength cones, and lowest for the short-wavelength cones. In contrast, photon absorption by rods (black) is reduced by ~20% because of the wave-guide properties of Müller cells.

Discussion

We showed here, using optical computational analysis, that white light incident upon the parafoveal retina of humans and upon the guinea pig retina, splits according to its spectral components by retinal Müller cells (Figs. 2 and 4 respectively). This was strongly supported by imaging experiments in the isolated guinea pig retina (Fig. 4). The Müller cell, acting as a wavelength-dependent optical fiber, concentrates the red-green part of the spectrum inside the cells, to reach the cones, while allowing blue-violet light to leak towards the surrounding tissue, to illuminate rods. The spectrum of light transmitted through the Müller cells, matches almost perfectly the absorption spectra of the medium- and long-wavelength human cone photoreceptors. At the same time the spectrum of light leaking outside the Müller cells matches the absorption spectrum of human rod photoreceptors. This leads to a significant gain, by a factor of ~7.5, in photon absorption by M- and L-cones, and by a factor of ~4 for the S-cones. This light concentration into cones is not impeding significantly light absorption in rods' outer segments, since most of the relevant light (wavelength between 400 nm and 500 nm) leaks out from the Müller cells towards the surrounding rods (Fig. 6).

The theoretical analysis on the benefits of Müller cells for light transmission across the retina in human parafoveal retina was supported by parallel theoretical and experimental analysis for the guinea pig retina.

However, the benefits of Müller cells for cone-mediated vision in the guinea pig retina is less apparent than in human because of the absorption spectra of guinea pig's cone visual pigments. Nevertheless, Müller cells increased photon absorption in M-cones by a factor of 5.1 and in S-cones by a factor of 2.1 without impeding significantly photon absorption (total reduction of 17%) in rods (see Supplementary Information).

Our conclusion that retinal Müller cells, via their wavelength-dependent light guiding properties, improve photon absorption by cones, and only slightly reduces photon absorption by rods is consistent with psychophysical tests in human observers which are based upon rates of photon absorptions by different types of photoreceptors.

In a typical Rayleigh color match, an observer matches a yellow light (589 nm) of fixed intensity to a mixture of green (545 nm) and red (670 nm) monochromatic lights by changing the green/red intensity ratio[36,37]. In this well-known experiment, the green/red ratio, needed for a match to the fixed yellow light, varies between foveal viewing and peripheral viewing. This ratio decreases as the spot size is increased to cover retinal regions outside the fovea[38]. This phenomenon has been explained by several mechanisms, including intrusion of rods, pre-retinal absorption by macular pigment, and changes in optical density of the cones' visual pigments between foveal cones and parafovea cones. The separation of colors by Müller cells in the human parafovea, which has been described here, can provide another simple mechanism to explain this result. According to our findings, Müller cells concentrate yellow light (589 nm) incident on the peripheral retina and propagate it directly onto the cones, leading to ~10-fold enhancement of the yellow light photon flux (Fig. 2a). Thus, in order to preserve color matching the green and red intensities (545 and 670 nm) need to be increased similarly. However, the Müller cells increase the intensity of the 545 nm green light by 9-fold and the 670 nm red light by only ~3-fold (Fig. 2a). Therefore, the observer needs to change the green/red ratio in a manner that will increase the red at the expense of the green, leading to a reduction in the green/red ratio[31].

In another elegant psychophysical research[38], human observers were asked to compare colors of monochromatic light between corneal illumination and trans-scleral illumination. One of the tests of that study compared the rod to cone excitation ratio for trans-scleral illumination compared to corneal illumination. It was reported that with trans-scleral illumination the rod to cone excitation ratio increased compared to the situation with corneal illumination. This observation is also consistent with our findings on the role of Müller cells in determining photon fluxes reaching the photoreceptors layer. With trans-scleral illumination, light reaches cones and rods equally, while with corneal illumination the Müller cells concentrate light towards the cones and at the same time reduce light reaching the rods, causing a decrease in rod to cone excitation ratio (Fig. 6).

Thus, the spectral separation of light by Müller cells provides a mechanism to improve cone-mediated day vision, with minimal interference with rod-mediated night vision. This is achieved by wavelength sorting of incident light by the Müller cells. Light of relevant wavelengths for cone visual pigments is directed towards the cones, while light of wavelengths more suitable for rod vision is allowed to leak outside the Müller cells towards the surrounding rods. This is a novel mechanism that needs to be considered when visual phenomena concerning cone- and rod-mediated vision are analyzed.

Methods

Full details on experimental procedures, analysis, and modeling are presented in the SI Methods.

Optical simulation analysis. To simulate light propagation through the human's and the guinea pig's retina, an optical model of the retina was reconstructed, based upon known optical properties of Müller cells and the neuronal layers of the retina[10,15,16]. The simulation method is based on a numerical solution of the scalar wave equation (Helmholtz equation). The most universal method for solving the latter for composite refractive index profiles is the Fast Fourier Transform Beam Propagation Method (FFT BPM), also called the split-step FFT BPM[18,19,21]. The algorithm is stable and provides a detailed and accurate description of the propagating electromagnetic field along the cells and their vicinity. We have written our algorithm in a MATLAB environment and tested it thoroughly[11]. We found it to match perfectly results for light propagation along cones[23,39,40,41], which were obtained and examined by other methods such as coupled mode theory[22,42,43,44].

Spectral imaging in the isolated retina. Spectral and spatial distributions of light were imaged in the guinea pig's isolated retina. All experiments were carried out according to the statement of "The Association for Research in Vision and Ophthalmology", and according to institutional guidelines. Male adult guinea pigs (500-700 gr) were sacrificed by an overdose (150 mg/kg) of sodium pentobarbital administered intraperitoneally. Freshly enucleated eyes were isolated, washed twice in PBS and circumferentially dissected posterior to the ora serrata. Anterior segment and vitreous were carefully removed. A fresh retinal preparation was mounted on the stage of an inverted meta-confocal microscope (LSM 510 Meta; Zeiss, Germany), with photoreceptors surface facing the objective. Light from a Halogen lamp, transmitted through an optical fiber, was collimated onto the retinal surface from the vitreal side. The transmitted light emanating from the retina was captured through the objective. For each field, the level of photoreceptors outer segments was identified prior to recording. We utilized the auto-fluorescence of photoreceptor outer segments[33]. Images of transmitted light were recorded at optical sections of 5 μm thick, spanning 50 μm above the last auto-fluorescent section. For each optical section, 27 distinct spectra were obtained at intervals of 10 nm width covering a 400 to 700 nm wavelength range.

Acknowledgements

We thank S. Shoham, R. Heinrich, N. Meitav, SG. Lipson, and E. Zemel for discussions. This research was partially supported by grants from the Israel Science Foundation; one to E.R. and one to I.P.

References

1. Wandell BA. *Foundations of vision*. Sinauer Associates (1995).
2. Wald G. The molecular basis of visual excitation. *Nature* **219**, 800-807 (1968).
3. Merbs SL, Nathans J. Absorption spectra of human cone pigments. *Nature* **356**, 433-435 (1992).
4. Masland RH. The fundamental plan of the retina. *Nat Neurosci* **4**, 877-886 (2001).
5. Dowling JE. The retina: an approachable part of the brain. (1987).
6. Ala-Laurila P, Greschner M, Chichilnisky E, Rieke F. Cone photoreceptor contributions to noise and correlations in the retinal output. *Nat Neurosci* **14**, 1309-1316 (2011).
7. Bialek W. Physical limits to sensation and perception. *Annu Rev Biophys Biophys Chem* **16**, 455-478 (1987).
8. Rieke F, Baylor DA. Origin and Functional Impact of Dark Noise in Retinal Cones. *Neuron* **26**, 181-186 (2000).
9. Luo D-G, Yue WW, Ala-Laurila P, Yau K-W. Activation of visual pigments by light and heat. *Science* **332**, 1307-1312 (2011).
10. Franze K, *et al.* Müller cells are living optical fibers in the vertebrate retina. *Proc Natl Acad Sci U S A* **104**, 8287-8292 (2007).
11. Labin AM, Ribak EN. Retinal glial cells enhance human vision acuity. *Phys Rev Lett* **104**, 158102 (2010).
12. Reichenbach A, Bringmann A. New functions of Müller cells. *Glia*, (2013).
13. Agte S, *et al.* Müller Glial Cell-Provided Cellular Light Guidance through the Vital Guinea-Pig Retina. *Biophysical Journal* **101**, 2611-2619 (2011).
14. Hecht S, Shlaer S, Pirenne MH. Energy, quanta, and vision. *The Journal of general physiology* **25**, 819-840 (1942).
15. Chao TI, *et al.* Comparative studies on mammalian Müller (retinal glial) cells. *J Neurocytol* **26**, 439-454 (1997).
16. Curcio CA, Sloan KR, Kalina RE, Hendrickson AE. Human photoreceptor topography. *J Comp Neurol* **292**, 497-523 (1990).
17. Okamoto K. Fundamentals of optical waveguides. (2006).
18. Thylen L. The beam propagation method: an analysis of its applicability. *Optical and quantum electronics* **15**, 433-439 (1983).
19. VanRoey J, van derDonk J, Lagasse PE. Beam-propagation method: analysis and assessment. *J Opt Soc Am* **71**, 803-810 (1981).
20. Drezek R, Dunn A, Richards-Kortum R. Light scattering from cells: finite-difference time-domain simulations and goniometric

measurements. *Applied Optics* **38**, 3651-3661 (1999).

21. Thylen L, Yevick D. Beam propagation method in anisotropic media. *Appl Opt* **21**, 2751-2754 (1982).
22. Snyder AW, Love JD. Optical waveguide theory. viii, 734 p. (1983).
23. Snyder AW, Pask C. The Stiles-Crawford effect--explanation and consequences. *Vision Res* **13**, 1115-1137 (1973).
24. Vohnsen B, Iglesias I, Artal P. Guided light and diffraction model of human-eye photoreceptors. *J Opt Soc Am A Opt Image Sci Vis* **22**, 2318-2328 (2005).
25. Vohnsen B. Photoreceptor waveguides and effective retinal image quality. *J Opt Soc Am A Opt Image Sci Vis* **24**, 597-607 (2007).
26. Beuthan J, Minet O, Helfmann J, Herrig M, Müller G. The spatial variation of the refractive index in biological cells. *Phys Med Biol* **41**, 369-382 (1996).
27. Bowmaker JK, Dartnall HJ. Visual pigments of rods and cones in a human retina. *J Physiol* **298**, 501-511 (1980).
28. Wyszecki G, Stiles WS. Color Science: Concepts and Methods, Quantitative Data and Formulae. *Color Science: Concepts and Methods, Quantitative Data and Formulae, 2nd Edition, by Gunther Wyszecki, WS Stiles, pp 968 ISBN 0-471-39918-3 Wiley-VCH, July 2000* **1**, (2000).
29. Stockman A, Sharpe LT. The spectral sensitivities of the middle-and long-wavelength-sensitive cones derived from measurements in observers of known genotype. *Vision Research* **40**, 1711-1737 (2000).
30. Roorda A, Williams DR. The arrangement of the three cone classes in the living human eye. *Nature* **397**, 520-522 (1999).
31. Solovei I, *et al.* Nuclear Architecture of Rod Photoreceptor Cells Adapts to Vision in Mammalian Evolution. *Cell* **137**, 356-368 (2009).
32. Kreysing M, Boyde L, Guck J, Chalut KJ. Physical insight into light scattering by photoreceptor cell nuclei. *Optics letters* **35**, 2639-2641 (2010).
33. Sparrow JR, Yoon KD, Wu Y, Yamamoto K. Interpretations of fundus autofluorescence from studies of the bisretinoids of the retina. *Investigative ophthalmology & visual science* **51**, 4351-4357 (2010).
34. Parry JW, Bowmaker JK. Visual pigment coexpression in guinea pig cones: a microspectrophotometric study. *Investigative ophthalmology & visual science* **43**, 1662-1665 (2002).
35. Krishnamoorthy V, Jain V, Cherukuri P, Baloni S, Dhingra NK. Intravitreal injection of fluorochrome-conjugated peanut agglutinin results in specific and reversible labeling of mammalian cones in vivo. *Investigative ophthalmology & visual science* **49**, 2643-2650 (2008).
36. He JC, Shevell SK. Variation in color matching and discrimination among deuteranomalous trichromats: Theoretical implications of small differences in photopigments. *Vision research* **35**, 2579-2588 (1995).
37. Rayleigh L. Experiments on colour. *Nature* **25**, 64-66 (1881).
38. Brindley G, Rushton W. The colour of monochromatic light when passed into the human retina from behind. *The Journal of Physiology* **147**, 204-208 (1959).
39. Westheimer G. Directional sensitivity of the retina: 75 years of Stiles-Crawford effect. *Proc Biol Sci* **275**, 2777-2786 (2008).
40. Westheimer G. Retinal light distributions, the Stiles-Crawford effect and apodization. *J Opt Soc Am A* **30**, 1417-1421 (2013).
41. Enoch JM. Optical properties of the retinal receptors. *JOSA* **53**, 71-85 (1963).
42. Marcos S, Burns SA. Cone spacing and waveguide properties from cone directionality measurements. *J Opt Soc Am A Opt Image Sci Vis* **16**, 995-1004 (1999).
43. Marcuse D. Radiation losses of step-tapered channel waveguides. *Appl Opt* **19**, 3676-3681 (1980).
44. Snyder AW. Excitation of waveguide modes in retinal receptors. *J Opt Soc Am* **56**, 705-706 (1966).

Supplementary Figures

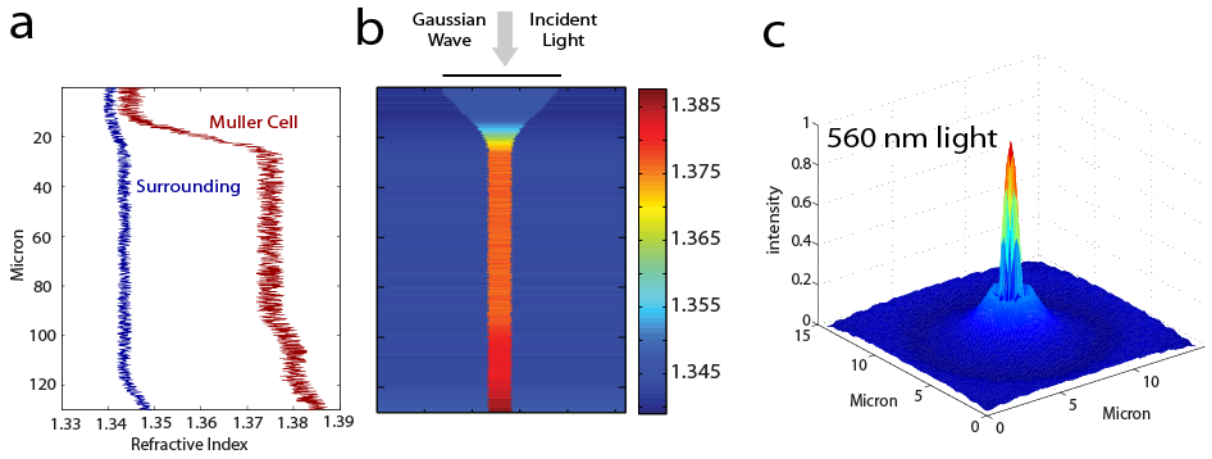

Supplementary Fig. 1: Light propagation simulation in the human retina. (a) Müller cell refractive index distribution (red) along the cell's length (130 µm), and the refractive profile of the surrounding area (blue). The cell's refractive index is higher than that of the surrounding along the entire retinal depth. (b) Simplified Müller cell structure and the corresponding refractive index. The cell's diameter and its refractive index are subject to small perturbations, which are included in the algorithm. The input light distribution has a gaussian shape with a plain wave front. (c) A characteristic intensity distribution for 560 nm light at the bottom of the Müller cell, after full propagation inside the cell and its surrounding.

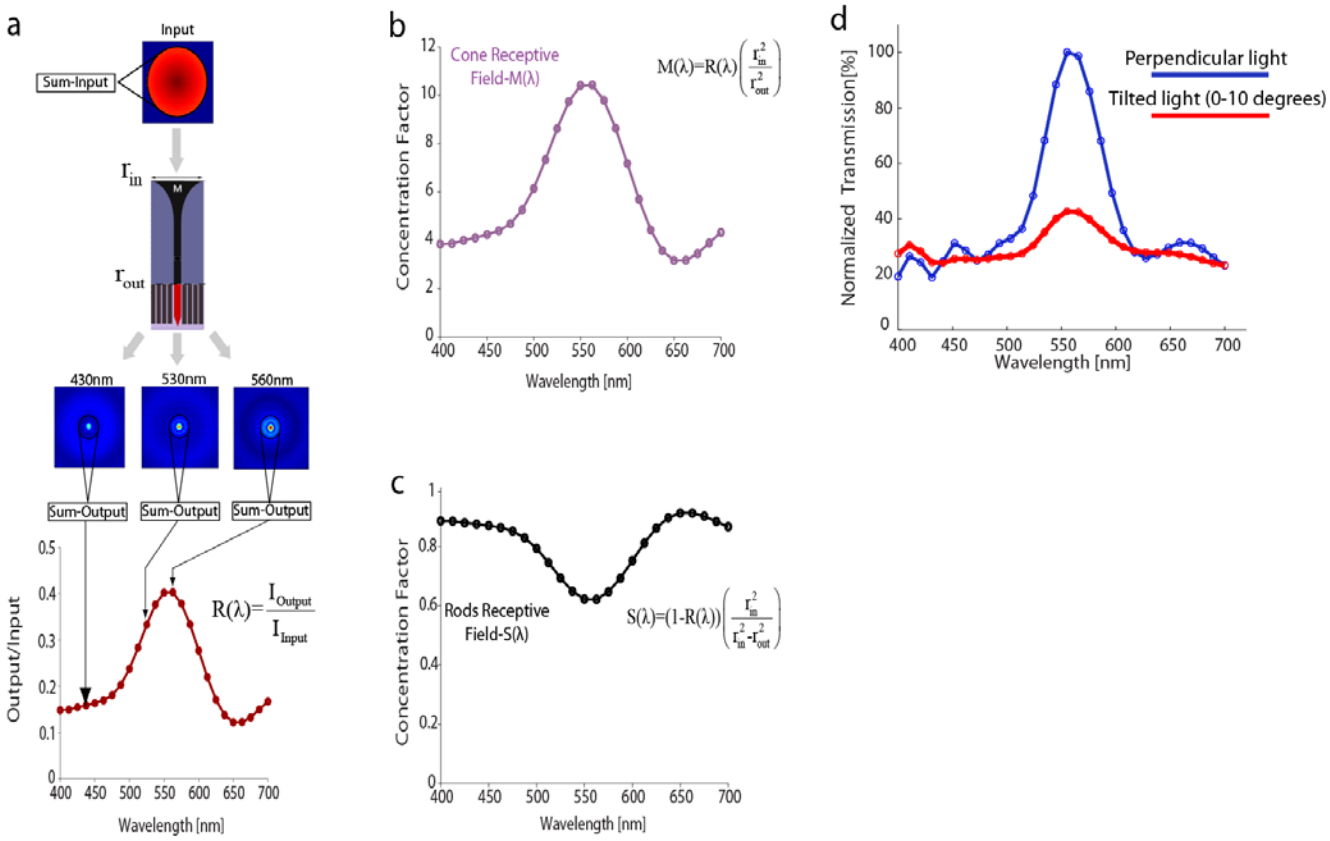

Supplementary Fig. 2: Light concentration by a Müller cell. (a) Calculating the ratio $R(\lambda)$ between the output and input light intensity. The light intensity is summed before incidence on the cell (input intensity) and after light propagation (output intensity), before the photoreceptors. The ratio between the inner and outer radius for the human Müller cell is r_{in}/r_{out} ~5-6. (b) Wavelength dependency of light concentration inside Müller cell $M(\lambda)$ obtained by Eq. S9. At 560 nm there is ~10-fold enhancement of light impinging upon the cone receptive field as a result of Müller cell concentration. (c) The corresponding wavelength dependency of light leaking outside Müller cell $S(\lambda)$ obtained by Eq. S12. (d) Transmission within the cell obtained for normal incidence (blue curve) and averaged tilted field, up to 10^{o} (red curve). The peak transmission is located in the same input wavelength.

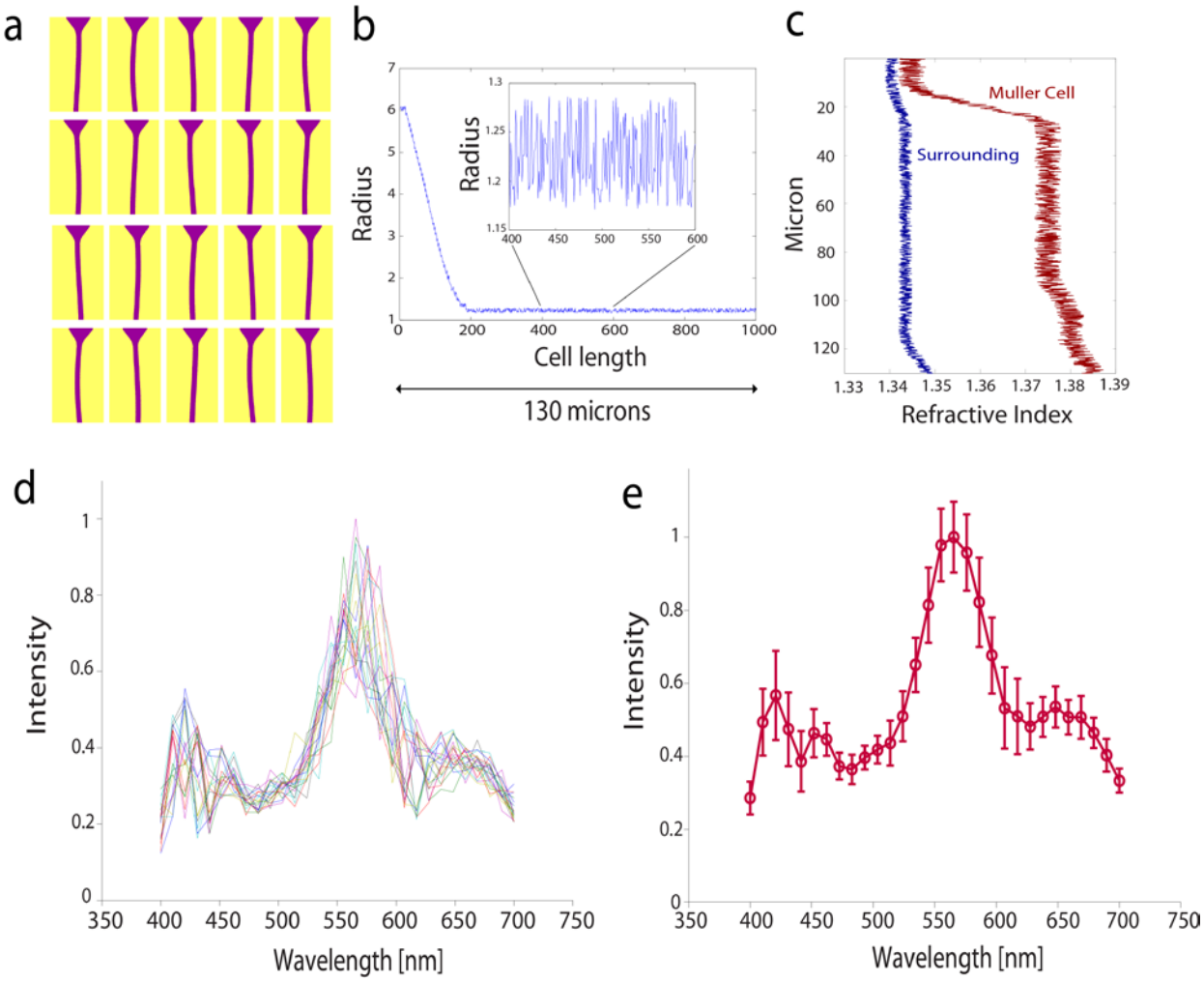

Supplementary Fig. 3: Testing the robustness of optical simulation. (a) Twenty cells realisations, possessing random bending along the longitudinal axis. (b) 5% random perturbations of the radius of one of the cells along its length (130 μm = 1000 numerical steps). (c) Perturbations of the refractive indices of surrounding neuronal layers and of Muller cells were added. (d) Spectra of light at the exit of all cells (N = 20) after illuminated by an abberated pupil. (e) Mean ± s.d. (N = 20) of the spectra of light at the exit of the Müller cells. The peak transmission is in the green, λ ~560 nm.

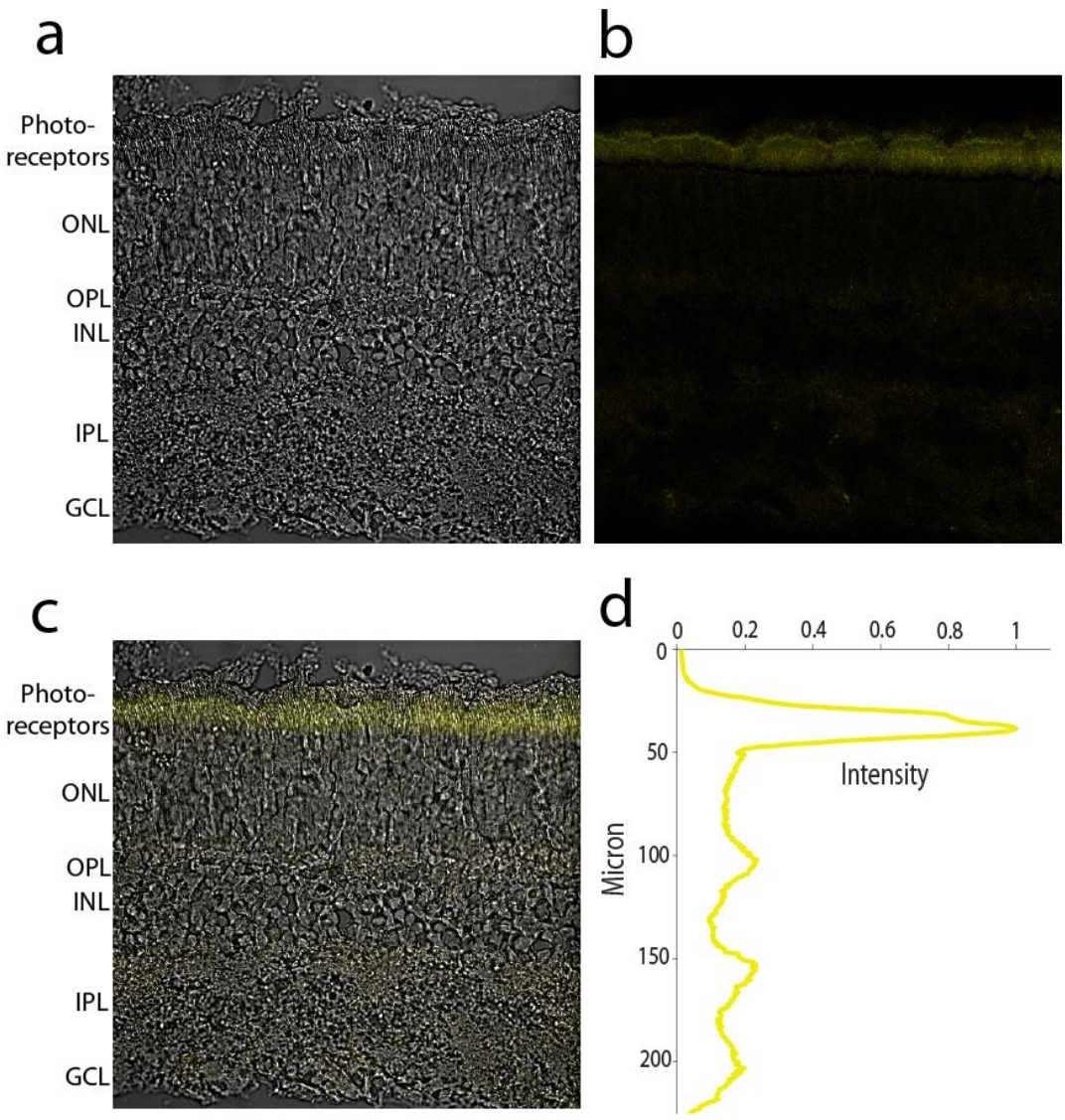

Supplementary Fig. 4: Identification of photoreceptors outer segments (POS) layer. POS were identified without exogenous labeling using the reflection mode of the LSM 510 meta-confocal microscope is demonstrated here for a rat retinal slice, 12 µm thick. The slice was illuminated with a 488 nm argon laser. (a) White channel represents the transmitted light, revealing retinal morphology. (b) The slice was illuminated with 488 nm argon laser and reflected light was measured, indicated by the yellow channel of the microscope (502±5 nm). (c) Overlay of both channels. (d) Profile of mean intensity of yellow channel along the retinal slice, demonstrating a significantly higher reflected light intensity from POS, allowing their identification.

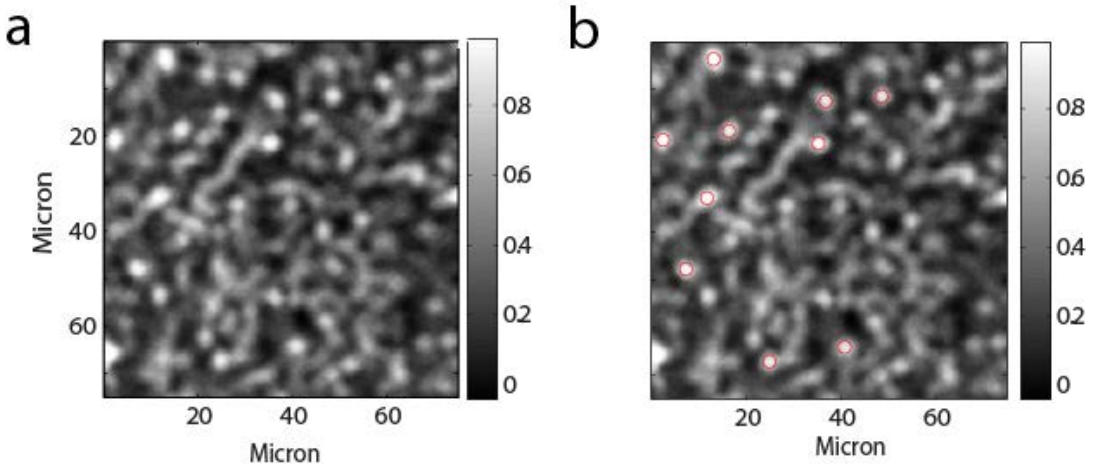

Supplementary Fig. 5: Spectral analysis of light transmission by Müller cells in the isolated guinea pig retina. (a) Spatial light distribution as recorded 50 µm above the layer of photoreceptors inner segment. Light is being tunneled inside distinct pathways. (b) Müller cells light tunneling areas were located by threshold determination, and the 10 cells of highest transmission were marked (red circles). The red circles mask was marked in the 26 remaining images. The 27-image stack corresponds to 27 distinct visible wavelengths (417 – 695 nm).

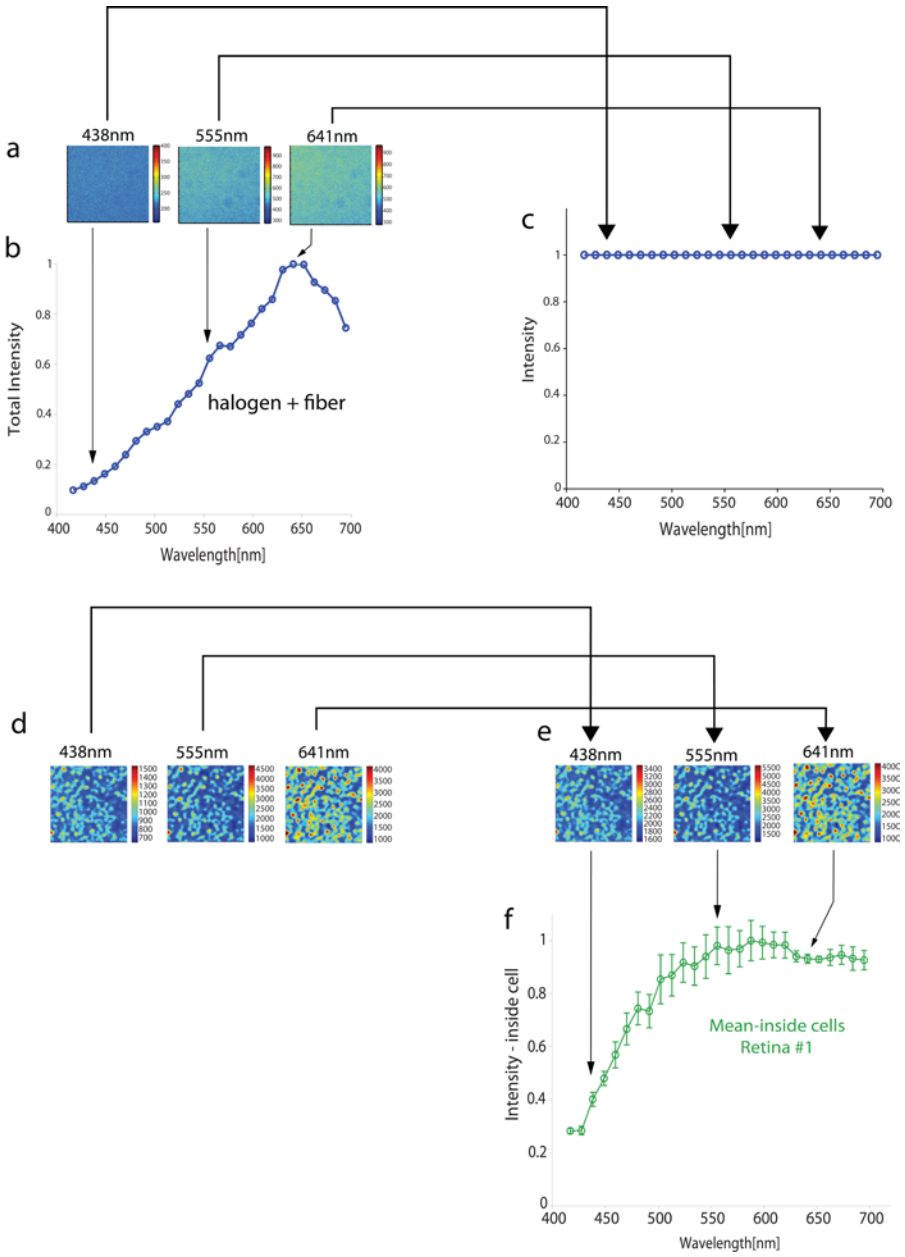

Supplementary Fig. 6: Normalisation scheme. (a) 27 Images recorded by the microscope lambda mode, where the halogen light source was projected by the optical fiber, without a sample. (b) Sum (over all pixels) for each of the 27 images is the spectrum of the halogen and fiber. (c) Image set after the normalisation scheme. (d) Three representative images of the 27 retinal transmission images recorded by the microscope lambda mode at the distal end of the Müller cells in the guinea pig retina. The halogen light source was projected by the optical fiber on the retinal surface. (e) The 27 images were normalised using the transformation weights derived for the light spectrum recorded without tissue. (f) Mean (± sd) of the spectral intensity inside Müller cells, studied in the guinea pig retina #1 after normalisation.

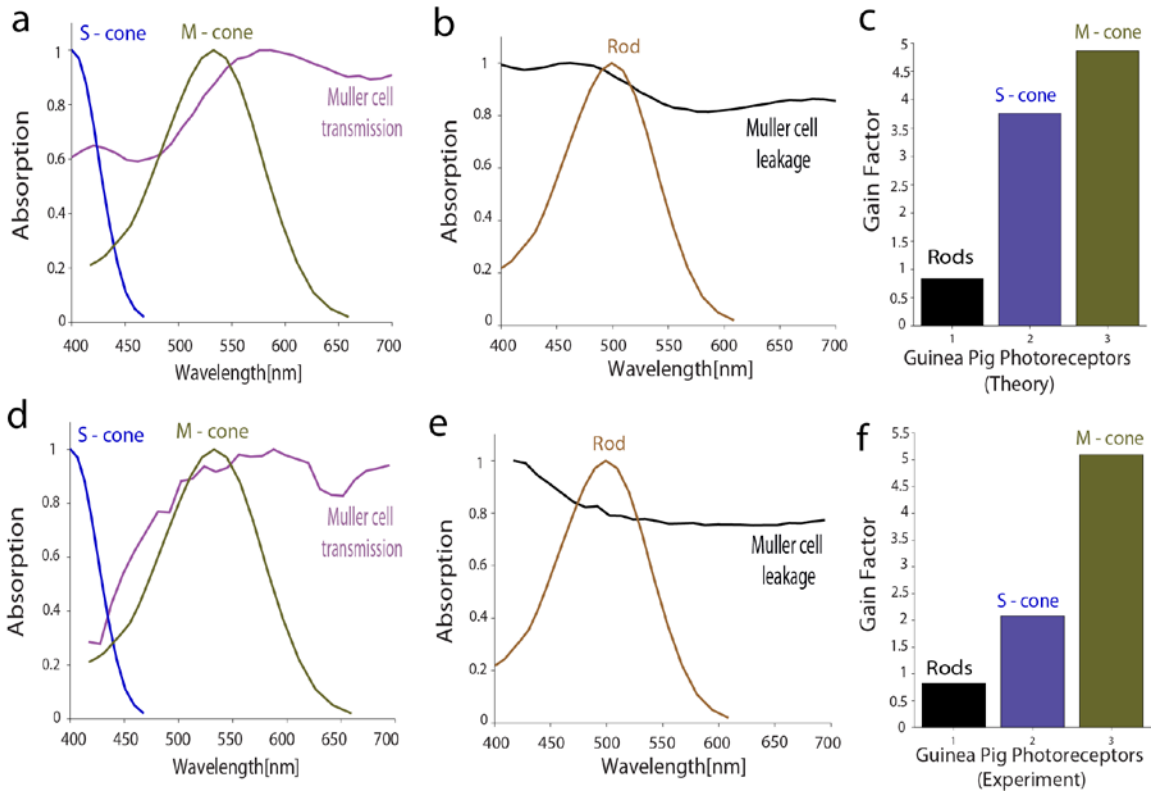

Supplementary Fig. 7: Gain of light absorption in the guinea pig photoreceptors (a) Absorption spectra of the guinea pig's S- and M-cones compared to the computational simulation of Müller cells spectral transmission onto cones. (b) Absorption spectra of the guinea pig's rods compared to spectral leakage from Müller cells to the rods. (c) Photoreceptors gain factor of light absorption due to theoretical separation of wavelengths by Müller cells. (d, e, f): The same as for (a, b, c) but with the experimentally measured spectral transmission and leakage in the guinea pig's retina.

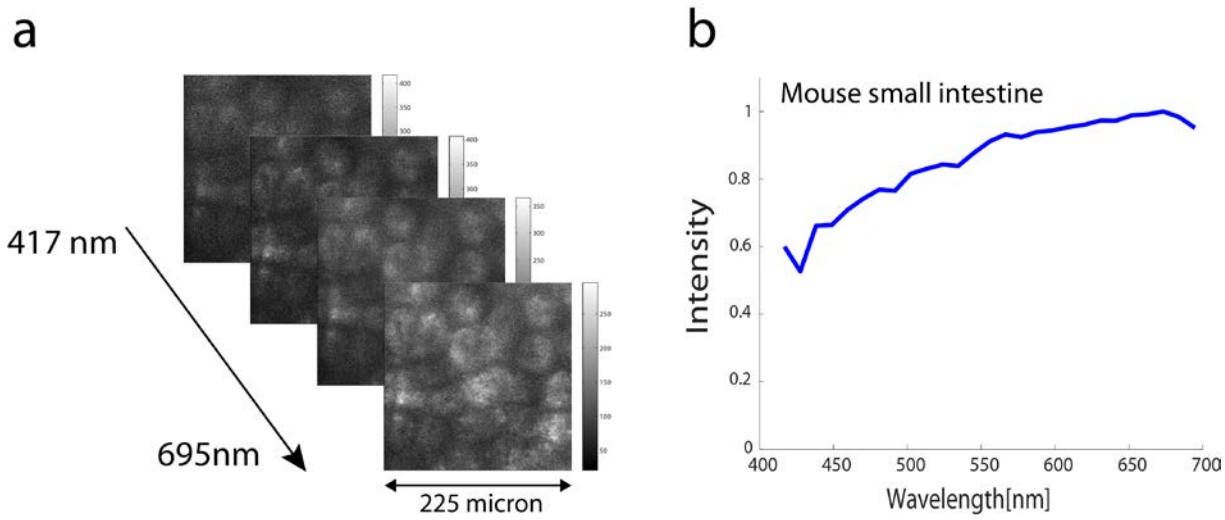

Supplementary Fig. 8: Comparison to other tissue. (a) Images of the mouse's small intestine in 27 wavelength bands. (b) Spectrum of light recorded after propagation through the tissue. The spectrum is obtained within the high transmission areas of the tissue (bright patches), by the same scheme used for the retina. This spectrum is markedly different from the retinal spectrum.

Supplementary Methods

Simulated light concentration by Müller cells

Due to the funnel-like shape of the Müller cell's endfoot in the vitreo-retinal junction, a Müller cell collects light from a large area and concentrates it into a smaller area in the distal end of the cell, onto one coupled cone (Supplementary Fig. 2a). The ratio between the diameter of its distal part (r_{out}) and the diameter of the endfoot (r_{in}) for the human Müller cell is ~1:5. In order to obtain the factor by which light intensity is multiplied due to the cell's light guiding properties, we calculated the light exit from the cell (output) relative to the light intensity impinging upon the endfoot (input). Thus, on the first step of the simulation we calculated the incident intensity I_{in}, which is given by a summation over the cell upper area ($r < r_{\text{in}}$, defined in Supplementary Fig. 2a)

$$I_{in} = \sum_{ij \in \{r < r_{in}\}} I_{ij}$$

Light arrives at Müller cells from the eye's pupil in a diffraction pattern, which is approximated by a uniform distribution in space (40 μm wide gaussian, much wider than the endfoot). Accordingly we calculated the intensity I_{out} after light propagation in the cell by a summation over the cell's outer area ($r < r_{\text{out}}$)

$$I_{\text{out}} = \sum_{ij \in \{r < r_{\text{out}}\}} I_{ij} .$$

We define the ratio between output and input intensity (Supplementary Fig. 2a) for a given wavelength as

$$R(\lambda) = \frac{I_{\text{out}}(\lambda)}{I_{\text{in}}} .$$

Throughout the simulation process, the input intensity I_{in} was constant for all wavelengths. Light density is determined by its intensity as well as by the area over which it is distributed. Therefore, the input light density is given by

$$\rho_{\text{in}} = \frac{I_{\text{in}}}{\pi r_{\text{in}}^2},$$

and the output light density is given by

$$\rho_{\text{out}} = \frac{I_{\text{out}}}{\pi r_{\text{out}}^2} .$$

Thus for a given wavelength, the gain in photon density as a result of Müller cell's light concentration, which we term as the concentration factor $M(\lambda)$, is given by the ratio of output and input density of light (Supplementary Fig. 2b)

$$M(\lambda) = \frac{\rho_{\text{out}}}{\rho_{\text{in}}} = \frac{I_{\text{out}}(\lambda)}{I_{\text{in}}} \left(\frac{r_{\text{in}}}{r_{\text{out}}} \right)^2 .$$

For the human Müller cell, $r_{\text{in}} / r_{\text{out}} \sim 5$, thus $M(\lambda) = 25 \cdot R(\lambda)$. Thus, for 560 nm light, $M \sim 10$, and there are $\times 10$ photons impinging on the cone receptive field as a result of Müller cell light concentration.

Since light absorption in the neural layers of the retina is negligible there is conservation of energy and $I_{\text{in}} = I_{\text{out}} + I_{\text{out\_surr}}$. Here $I_{\text{out\_surr}}$ is the intensity of light leaking out of the Müller cell during propagation, into the surrounding area, and finally being incident on the rod photoreceptors. Now we define, in a similar manner, the light density in the surrounding area

$$\rho_{\text{out\_surr}} = \frac{I_{\text{in}} - I_{\text{out}}}{\pi(r_{\text{in}}^2 - r_{\text{out}}^2)}.$$

Thus, for a given wavelength, the light concentration factor in the Müller cell's surrounding area $S(\lambda)$ (Supplementary Fig. 2c) is given by

$$S(\lambda) = \frac{\rho_{\text{out\_surr}}}{\rho_{\text{in}}} = [1 - R(\lambda)]\frac{r_{\text{in}}^2}{r_{\text{in}}^2 - r_{\text{out}}^2}$$

For 560 nm light S ~ 0.6, thus there are $\sim \times 0.6$ photons impinging the rod receptive fields as a result of Müller cell light concentration (a 40% reduction of light intensity for rods, less at shorter wave lengths).

When light enters the pupil away from its center, it reaches the retina as a tilted wavefront, rather than perpendicularly. At night time, the pupil dilates up to 8 mm, and with an average eye length of 23 mm, the maximum incidence angle with respect to the retina is $\sim 10^0$. Therefore, we calculated also the average transmission of light in the waveguide cells with an incident slant of up to 10^0, and found it to have the same wavelength for peak transmission (Supplementary Fig. 2c, red curve). The relative intensity is lower, as can be expected when the leakage increases as a result of higher incident angle.